

## UNSTABLE PLANETARY SYSTEMS EMERGING OUT OF GAS DISKS

SOKO MATSUMURA<sup>1</sup>, EDWARD W. THOMMES<sup>1,2</sup>, SOURAV CHATTERJEE<sup>1</sup> AND FREDERIC A. RASIO<sup>1</sup>

*Draft version March 15, 2009*

### Abstract

The discovery of over 300 extrasolar planets allows us to test our understanding of formation and dynamics of planetary systems statistically via numerical simulations. Traditional N-body simulations without a gas disk have successfully reproduced the eccentricity ( $e$ ) distribution of the observed systems, by assuming that the planetary systems are relatively compact when the gas disk dissipates, so that they become dynamically unstable within the stellar lifetime. However, such studies cannot explain the small semimajor axes  $a$  of extrasolar planetary systems, if planets are formed beyond the ice line, as the standard planet formation theory suggests.

In this paper, we perform numerical simulations of multi-planet systems in dissipating gas disks to (1) verify the initial conditions of the N-body simulations, and (2) constrain the initial conditions which reproduce both the observed  $a$  and  $e$  distributions simultaneously. We find that the planetary systems tend to be dynamically “inactive” when the gas disks dissipate, and therefore the initial conditions of the N-body simulations may not be recovered. We also find that the eccentricity damping in the gas disk may need to be inefficient, possibly due to the saturation of corotation torques, to reproduce both  $a$  and  $e$  distributions satisfactorily.

*Subject headings:* methods: numerical, n-body simulations, planetary systems: protoplanetary disks, formation, planets and satellites: formation, general

### 1. INTRODUCTION

Out of over 280 planetary systems discovered so far, about 12.5% are known to be multiplanet systems (<http://exoplanet.eu/>). Since the observed orbital parameters of multiplanet systems are statistically indistinguishable from those of single-planet systems (Udry & Santos 2007), currently known single-planet systems may possess, or may have possessed, undetected planetary companion(s). In fact, recent observations have started revealing that many of the detected planets are accompanied by a planet on a further orbit (e.g. Wittenmyer et al. 2007; Wright et al. 2007). It will become increasingly more important to understand the formation and evolution of such multiplanet systems, which can explain the observed properties of these systems.

Recent N-body numerical simulations of planetary systems *without* a gas disk demonstrated that dynamical instabilities occurring in the multiplanet systems, which are characterized by orbital crossings, collisions, and ejections of planets, could increase planetary eccentricities ( $e$ ) efficiently (Rasio et al. 1996; Weidenschilling & Marzari 1996). These studies successfully reproduced the observed eccentricity distribution of extrasolar planets (Ford & Rasio 2007; Chatterjee et al. 2008; Jurić & Tremaine 2008, from here on C08, and JT08, respectively.)

Such N-body simulations also suggest that the planet–planet interactions alone cannot explain small semimajor axes ( $a$ ) of the observed planets, *if* giant planets are formed beyond the ice line as expected from the standard planet formation theory. This is not very surprising since planet–planet interactions are not particularly efficient in

shrinking the planetary orbits.

The planet-disk interactions, on the other hand, are known to decrease semi-major axes of planets efficiently (Ward 1997). Adams & Laughlin (2003) and Moorhead & Adams (2005) studied the evolution of two-planet systems embedded in the inner cavity of a disk. They applied a parameterized semimajor axis damping force to the outer planet, and investigated the evolution of two-planet systems as the outer planet approaches the inner one. They found that their model naturally led to dynamical instability, and reproduced the overall trend of the observed  $a$ - $e$  scattered plot.

In this paper, we numerically study the evolution of three- and more planet systems in a dissipating gas disk, and constrain the “initial” conditions of planetary systems which can reproduce the  $a$  and  $e$  distributions simultaneously. We choose three different initial setups: 1) planets in an inner cavity of a disk, 2) planets fully embedded in a gas disk with an efficient eccentricity damping, and 3) planets fully embedded in a gas disk with less efficient eccentricity damping. For the third case, an effect of the saturation of corotation resonances is taken into account, while for the second case, we neglect this effect. In Section 2, we discuss possible paths to reproduce both  $a$  and  $e$  distributions of the observed planets. We introduce our numerical methods in Section 3, and show an example run in Section 4. In Section 5-7, we present the results for different initial setups. Finally, we summarize our work in Section 8.

### 2. SCENARIOS FOR EVOLUTION OF PLANETARY SYSTEMS

In this section, we briefly discuss three possible scenarios to reproduce both  $a$  and  $e$  distributions simultaneously. As we mentioned in the last section, the planet–planet interactions are efficient in exciting the planetary eccentricities, but they are not particularly good in de-

<sup>1</sup> Department of Physics and Astronomy, Northwestern University, Evanston, IL 60208, USA

<sup>2</sup> University of Guelph, Guelph, ON, Canada

creasing the planetary semi-major axes. On the other hand, the planet-disk interactions help planets to migrate inward, but they tend to damp planetary eccentricities. Therefore, we can expect that the  $a$  distribution of planetary systems is well-determined by the time the gas disk dissipates ( $\tau_{GD}$ ), while the eccentricity distribution is determined depending on when the dynamical instability sets in ( $\tau_{dyn}$ ) and active planet-planet scattering events occur.

Generally speaking, there are 3 possible scenarios which can lead to the observed  $a$ - $e$  distributions, depending on the onsets of dynamical instabilities — (1) the dynamical instability sets in *after* the gas disk dissipates ( $\tau_{GD} \lesssim \tau_{dyn}$ ), (2) the dynamical instability sets in *before* the gas disk is gone ( $\tau_{GD} \gtrsim \tau_{dyn}$ ), and (3) the dynamical instability sets in both before and after the gas disk’s dissipation.

For the first case, most planets stay on nearly circular orbits while the gas disks are around, because the disk’s eccentricity damping is strong enough. If this is the dominant scenario, the dynamical instability must occur after the gas disk’s dissipation for most systems to recover the observed  $a$ - $e$  distribution. This is the underlying assumption for all the previous N-body simulations which successfully explained the observed  $e$  distribution.

For the second case, most planetary systems become dynamically unstable, and planetary eccentricities get excited while the gas disks are around. If this is the dominant scenario, the disk’s eccentricity damping has to be weak enough to leave these eccentricities high to recover the  $a$ - $e$  distribution.

The third case is similar to the second case, but the disk’s eccentricity damping is efficient and planetary eccentricities are significantly damped after the first episode of dynamical instability. If this is the dominant scenario, disks must help convergent migration between planets, so that there will be another episode of dynamical instability.

In the following sections, we refer to each of these cases as “late instability”, “early instability”, and “multiple instability” cases, respectively.

### 3. NUMERICAL METHODS AND INITIAL CONDITIONS

To simulate multiplanet systems in gas disks, we use a hybrid code which combines the symplectic N-body code SyMBA (Duncan et al. 1998) with a one-dimensional gas disk evolution code (Thommes 2005). SyMBA utilizes a variant of the so-called mixed-variable symplectic (MVS) method (Wisdom & Holman 1991), which treats the interaction between planets as a perturbation to the Keplerian motion around the central star, and handles close encounters between bodies with a force-splitting scheme which has the properties of an adaptive timestep (Duncan et al. 1998). When the bodies are well-separated, SyMBA has the speed of the MVS method, while during the close encounters, the timestep for the relevant bodies is recursively subdivided.

On the other hand, the gaseous disk evolves both viscously and via gravitational interaction with planets, according to a general Navier-Stokes equation. Following the standard prescription by Lin & Papaloizou (1986), the gas disk is divided into radial bins, which represent disk annuli with azimuthally and vertically averaged disk properties like surface mass density, tempera-

ture, and viscosity. Viscous evolution of the disk is calculated by using the standard alpha viscosity prescription (Shakura & Sunyaev 1973), while the disk-planet interactions modify the disk evolution via the torque density formulated in Ward (1997) (see also Menou & Goodman 2004). The calculated torque density is used in turn to determine the migration rates of planets.

In our simulations, a disk stretches from 0.02 to 100 AU, and the orbital evolution of planets is followed down to 0.02 AU. The timestep of simulations is typically 0.05 yr, which ensures a reasonable orbital resolution down to  $\sim 0.2$  AU.

#### 3.1. Gas Accretion onto a Planet

In the above code, we could follow the evolution of planetary systems as they gravitationally interact with each other, migrate, and open gaps in the disk. In reality, planets are also expected to clear the gas annuli between them as they grow by accreting gas from the surrounding disk. This is likely to lead to convergent migration, and possibly dynamical instability. Therefore, we also take account of gas accretion onto a planet.

Once a planet becomes massive enough to open a gap in the disk, the gas accretion rate is controlled by how quickly the disk can supply gas to the planet, rather than how quickly the planet can accrete gas (Bryden et al. 2000; Tanigawa & Watanabe 2002). Since all the planets in our simulations are more massive than the Neptune, they are expected to have circumplanetary disks, from which they accrete. Although our code does not resolve such disks, we can mimic the accretion effect by adopting the results of hydro simulations. These simulations have shown that giant planets tend to accrete gas within the radius of  $\sim 2R_{hill}$  from the subdisk on the accretion timescale of (D’Angelo et al. 2003)

$$\tau_{subdisk} = \frac{M_p}{\dot{M}_p} \quad (1)$$

$$\log \left( \frac{\dot{M}_p}{M_E \text{ yr}^{-1}} \right) = \left( 18.47 + 9.25 \log \left( \frac{M_p}{M_*} \right) + 1.266 \log \left( \frac{M_p}{M_*} \right)^2 \right) (2)$$

Throughout this paper, we assume that all planets accrete gas on this timescale. The code used here is identical to the one in Matsumura et al. (2009). Note that the increase in planetary mass via accretion is very small in our simulations.

#### 3.2. Eccentricity Damping

We damp the planetary eccentricities on the following timescale (e.g. Kominami & Ida 2004):

$$\tau_{edamp} = -\frac{e_p}{\dot{e}_p} = \frac{1}{K_e} \left( \frac{h}{r} \right)^4 \left( \frac{M_*^2}{M_p \Sigma r^2} \right) \Omega^{-1}. \quad (3)$$

Here,  $K_e$  governs the damping efficiency, and we define this parameter by following the approach of Goldreich & Sari (2003), and normalizing it so that  $K_e = 1$  when there is no saturation of the corotation resonances,

$$K_e = \frac{1}{0.046} [1.046 F(p) - 1]. \quad (4)$$

In this equation,  $F(p)$  is the saturation function of corotation torques which is numerically evaluated by Ogilvie & Lubow (2002) and interpolated by

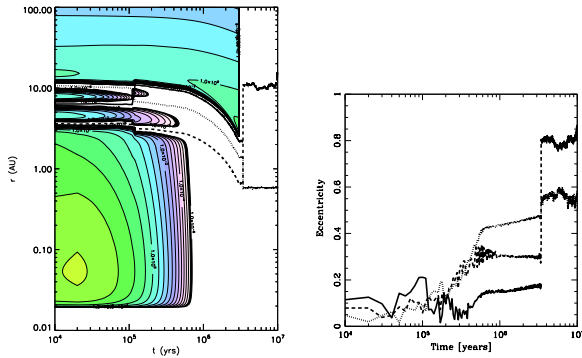


FIG. 1.— Evolution of a three-planet system. Left: Semi-major axis evolution of three planets. Solid, dashed, and dotted curves represent planets with  $1.2$ ,  $0.8$ , and  $1.8M_J$ , respectively. Also plotted are surface mass density contours. The density decreases in the order of rainbow colors, from red to purple. After the scattering event at  $\sim 10^5$  yr, planets are trapped in 6:3:1 MMRs until one of the planets ( $1.2M_J$ ) gets ejected out of the system after gas disk dissipation. Right: The corresponding eccentricity evolution for three planets.

Goldreich & Sari (2003) as

$$F(p) \simeq \frac{(1 + 0.65 p^3)^{5/6}}{(1 + 1.022 p^2)^2} \quad (5)$$

$$p \sim \left(\frac{r}{h}\right)^{2/9} \left(\frac{M_*}{M_p}\right)^{1/9} \frac{e_p}{\alpha^{1/9}}. \quad (6)$$

For  $K_e = 1$ , the corotation torques are not saturated, and fully contribute to the eccentricity damping, while for the other extreme  $K_e = 0$ , the effect of corotation torques are negligible, and there is no damping. For simplicity, we don't take account of the eccentricity excitation effect due to the disk–planet interaction. Therefore, the eccentricity excitation seen in our simulations is solely due to the effect of planet–planet interactions. Note, however, that numerical simulations show that the disk–planet interactions typically lead to  $e < 0.2$  (e.g. D'Angelo et al. 2006), and therefore may not be able to explain planets with high eccentricities. We assume  $K_e = 1$  in Section 4-6, and discuss other cases in Section 7.

### 3.3. Disk Dissipation Timescale

C08 suggested that the dynamical instability occurs more frequently as the disk mass decreases. Generally, the lifetime of gas disks is estimated to be  $1 - 10$  Myr (e.g. Hillenbrand 2005; Sicilia-Aguilar et al. 2006), but the mechanism of the final dispersal of disks is not well-understood.

Observations suggest that such a timescale is rather short,  $\sim 10^5$  yr (e.g. Simon & Prato 1995). Since the viscous accretion timescale of a disk is longer than this, currently the most promising mechanism to explain the rapid dispersal of disks is photoevaporation, which can remove a disk within  $10^5 - 10^6$  yr in favorable cases (Matsuyama et al. 2003; Alexander et al. 2006). Here, we simply treat the gas disk dissipation time as a parameter, and assume that the entire disk is removed exponentially once  $\tau_{GD}$  is reached. In a Jupiter-mass disk, this disk removal timescale is about  $10^5$  yr.

## 4. AN EXAMPLE RUN

Fig. 1 shows an example run of our simulations. Here, the initial planetary masses are  $M_1 = 1.2M_J$ ,  $M_2 =$

$0.8M_J$ , and  $M_3 = 1.8M_J$  for solid, dashed, and dotted curves, respectively. Subscripts are in order of initial distance from the central star throughout the paper. Since we start with almost fully-grown planets, the initial gas disk mass is chosen to be  $0.71M_J$ , which corresponds to the mass of a minimum mass solar nebula (MMSN) type disk ( $\Sigma = 10^3(a/\text{AU})^{-1.5} \text{ g cm}^{-2}$ ) stretching from  $0.02$  to  $100$  AU, and evolved for  $7$  Myr under the disk viscosity  $\alpha = 5 \times 10^{-3}$  without planets. At the start of the simulation, all planets are fully embedded in a gas disk, and have no gaps.

Initially, planets are at  $5$ ,  $7$ , and  $10$  AU, for  $M_1$ ,  $M_2$ , and  $M_3$ , respectively. The initial distances between these planets correspond to  $3.8$  mutual Hill radii. Due to the proximity of these planets, they gravitationally scatter off each other within  $10^4$  yr after the simulation starts. This leads to orbital crossing of the inner two planets, leaving  $M_2$ ,  $M_1$ , and  $M_3$  at  $3.6$ ,  $6.3$ , and  $10.7$  AU at  $10^4$  yr, respectively. However, this orbital crossing does not result in dynamical instability of the system because of the presence of a sufficiently massive disk. Once planets reach these marginally stable orbits, they open gaps, and accrete gas within the radius of  $2R_{hill}$  on a sub-disk accretion timescale (See Eq. 1, and 2). As can be seen in the left panel of Fig. 1, gas accretion onto the planet removes all gas between planets in  $\lesssim 10^5$  yr. For the outer two planets ( $M_1$ , and  $M_3$ , or solid and dotted curves), the gravitational interaction is strong enough to scatter them with each other as the disk annulus between them is removed at around  $10^5$  yr. This crossing does not lead to dynamical instability either, thanks to the residual disk. Instead, they are trapped in the 3:1 Laplace resonance — the inner two planets (dashed and dotted curves) are trapped in the 3:1 MMR, while the outer two planets (dotted and solid curves) are trapped in the 2:1 MMR. As a consequence, their eccentricities increase steadily until  $\sim 5 \times 10^5$  yr, when the gas annulus between the inner two planets disappears, and all planets share one gap. Then, the inner disk, which is cleanly separated from the outer disk and therefore cannot be replenished, accretes toward the central star rather quickly in  $1 - 2 \times 10^5$  yr. Planet migration speeds up once the inner disk disappears, because planets only receive the negative torque from the outer disk. Since they are in the 6:3:1 Laplace resonance, they migrate in concert until the gas disk is exponentially removed at  $3$  Myr. The disk removal leads to dynamical instability with ejection of the outermost (initial innermost) planet (solid curve) and orbital crossing between the inner two planets (dashed and dotted curves). The ejection of a planet leaves the others on eccentric orbits with  $a \simeq 0.6$  AU and  $e \simeq 0.6$  for  $M_3$ , and  $a \simeq 15$  AU and  $e \simeq 0.85$  for  $M_2$ .

In short, for this particular example,  $\tau_{GD} \lesssim \tau_{dyn}$ , and the planetary system becomes dynamically unstable soon after the gas disk dissipation, which leads to the ejection of a planet, and the two remaining eccentric planets on widely separated orbits.

## 5. THREE-PLANET SYSTEMS IN A DISK CAVITY

In this subsection, we investigate three-planet systems which are surrounded by a residual outer gas disk. This is a similar setup to Adams & Laughlin (2003) and Moorhead & Adams (2005), but we use three-, instead of two-planet systems, and self-consistently calculate the

evolution of a disk and planetary orbits, instead of applying a parameterized damping force. The underlying assumption of this setup is that, after three planets are formed, they accreted all gas in the disk annuli between them, and shared a gap, while the inner disk, which was separated from the outer disk by these three planets sharing the gap, lost its gas reservoir, and accreted onto the central star on a viscous timescale. Such configurations are commonly seen in multiple planet formation simulations (Thommes et al. 2008).

### 5.1. Initial Conditions

We run three sets of simulations with different disk properties, where each set consists of 100 three-planet systems.

The outer disk is assumed to extend from 15 to 100 AU, with the initial surface mass density of  $\Sigma = \Sigma_0(a/AU)^{-3/2}$  with  $\Sigma_0 = 50, 40,$  and  $30 \text{ g cm}^{-2}$  (Set S50, S40, and S30, respectively). The corresponding initial masses in the outer disk are  $0.45, 0.36,$  and  $0.27M_J$  for each of these sets, respectively. The gas disk dissipation time is chosen randomly between 2 – 5 Myr for each system. The initial conditions for disks are summarized in Table 1.

For planetary systems, we define their initial properties following C08. In this model, the planetary mass  $M_p$  is determined by assuming that each planetary core accretes all gas within a “feeding zone” extending over  $\Delta = 8R_{hill, core}$ , and centered on the core:

$$M_p = 2\pi a \Delta \Sigma + M_{core}.$$

Here, the core mass  $M_{core}$  is randomly chosen from a uniform distribution over  $1 - 10M_E$  (where  $M_E$  is the Earth mass), and the core’s Hill radius is defined as  $R_{hill, core} = (M_{core}/(3M_*))^{1/3}a$ . The size of the feeding zones is a typical distance between planetary embryos (Kokubo & Ida 2002).

As in C08, the semimajor axes are chosen so that the distance between planets is scaled with  $K = 4.4$  times the Hill radius of the  $i$ -th planet:

$$a_{i+1} - a_i = K R_{hill, i},$$

with  $a_1 = 3AU$ . We fix the initial semimajor axis of the innermost planet following the common assumption that giant planets form beyond the “ice line”, where the solid density is higher due to the condensation of icy and/or carbonaceous material (Lewis 1974; Lodders 2004). From this prescription, we obtain planets with mass ranging over  $0.4 - 1.2M_J$ , between 3 to 5.2 AU.

All the other initial orbital parameters are chosen randomly from the uniform distribution in the following ranges: eccentricity  $e = 0 - 0.1$ , inclination  $i = 0 - 10$  degrees and uniform in  $\cos i$ , as well as phase angles  $0 - 360$  degrees.

### 5.2. Agreement with $a$ and $e$ distributions

In this subsection, we compare the  $a$  and  $e$  distributions of each set of simulations with the observed distributions, and discuss their overall evolutionary trends.

The outcomes of the simulations are summarized in Table 2, which shows the ejection, collision, and merger rates for each set of runs. Throughout this paper, we define that planets are “ejected” out of the system when

their orbital radii become larger than some predefined value, typically 1000 AU. Also, we assume that planets are “collided” with the central star, when their orbital radii become smaller than the inner disk radius 0.02 AU. Planets are labeled as “merged” when they collided with each other. Generally, a high collision rate implies an efficient planet migration in the gas disk, and high ejection, or merger rates indicate that the systems are dynamically unstable.

From Table 2, we can see that the ejection rates become higher after the gas disk dissipation for all the sets. However, for Set 9 and 10, the ejection rates before  $\tau_{GD}$  are less than, but comparable to, those after  $\tau_{GD}$ . Therefore, it is inferred that, for the massive disk cases (Set S50 and S40), the gas disk helped convergent migration between planets, and some planetary systems became dynamically unstable before  $\tau_{GD}$ . The high ejection rates after  $\tau_{GD}$  indicates that some of the planetary systems may have migrated convergently again, after the scattering events. Thus, we classify Set S50 and S40 as “multiple instability” cases. On the other hand, for the lightest disk (Set S30), the ejection rate is markedly higher *after* gas dissipation ( $\tau_{GD} \lesssim \tau_{dyn}$ ), and therefore we classify this case as a “late instability” case.

In Fig. 2, the observed eccentricity distribution (orange, or light grey histograms) is compared with the simulated results (blue, or dark histograms) at gas dissipation time  $\tau_{GD}$  (left panels), and at the end of the simulations, 100 Myr (right panels), for these sets. Two things are immediately clear from the figure — (1) as expected from a significant ejection rate *before*  $\tau_{GD}$ , some planets are very eccentric at  $\tau_{GD}$ , especially for Set S50 and S40, and (2) as expected from a significant ejection rate *after*  $\tau_{GD}$ , there is a clear  $e$  evolution between  $\tau_{GD}$  and 100 Myr for all sets.

These statements can be quantified by the Kolmogorov-Smirnov (K-S) test. We perform K-S tests against the null hypothesis that two arbitrary distributions are drawn from the same underlying distribution, and quote the significance level probabilities in Table 3. We choose to reject the null hypothesis for  $P < 0.1$ . For the K-S test, we choose planets between 0.2 and 6 AU, where the lower limit comes from the resolution limit of our simulations (see Section 3), while the upper limit is roughly the current maximum orbital radius of a planet detected by radial-velocity observations.

As an example, the K-S tests for the simulated results at  $\tau_{GD}$  and 100 Myr indicate that their  $e$  distributions are significantly different from each other, and thus all of these sets underwent a significant  $e$  evolution between these periods of time.

The K-S test, however, should be used with care. For example, the K-S test also assesses that the null hypothesis cannot be rejected for the observed distribution and the final distribution for Set S50, while these two distributions clearly look different from each other in Fig. 2. This is likely because the distribution is not continuous near the center for this set, and the K-S test is not as sensitive at tails of a distribution.

In Fig. 3, the corresponding plots for semimajor axis are shown. Again, two things are immediately apparent — (1) there is no significant  $a$  evolution between  $\tau_{GD}$  and 100 Myr, and (2) compared to the observed  $a$  distribu-

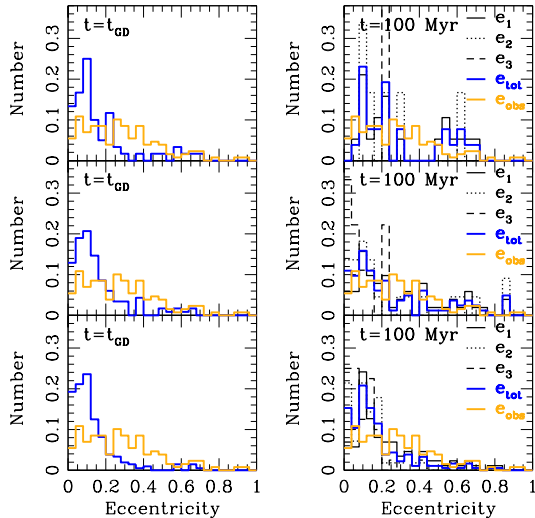


FIG. 2.— Eccentricity distributions for Set S50, S40, and S30 (from top to bottom) at  $\tau_{GD}$  (left panels) and 100 Myr (right panels). Due to the efficient eccentricity damping, there are few planets with eccentricity larger than 0.3 at  $\tau_{GD}$ , while there are more planets with high eccentricity at 100 Myr due to planet-planet scattering.

tion, all of these sets (especially Set S50, and S40) overproduce planets with small semi-major axes. Indeed, the K-S tests for simulated results at  $\tau_{GD}$  and 100 Myr show that we cannot decline the null hypothesis at our chosen rejection level. This supports the expectation that planet migration in a gas disk mostly determines the final semi-major axis distribution. The K-S tests also indicate that the “final” semimajor axis distributions for all of these sets disagree with the observed distribution.

In summary, we find that, in our simulations, it is difficult to match both the semimajor axis and eccentricity distributions simultaneously, assuming that three planets are initially in an inner cavity of a gas disk, and that the eccentricity damping is efficient. When a gas disk mass is low (Set S30), the effect of convergent migration is weak, and the systems tend to stay relatively stable until the gas disk dissipates ( $\tau_{GD} \lesssim \tau_{dyn}$ , i.e. late damping case). However, in such a case, the dynamical instability occurring after  $\tau_{GD}$  is not effective enough to produce high eccentricity planets. On the other hand, when a gas disk is sufficiently massive (Set S50 and S40), the convergent migration is efficient enough to start the dynamical instability while a gas disk is still around ( $\tau_{GD} \gtrsim \tau_{dyn}$ ). The eccentricity obtained during this period is mostly damped due to the disk-planet interactions (see left panels of Fig. 2). However, the disk is still massive enough to converge planetary orbits again so that the dynamical instability occurs after the gas disk is gone. These “multiple instability” cases can efficiently excite planetary eccentricities, but overproduce the planets with small semi-major axes.

## 6. EFFICIENT ECCENTRICITY DAMPING CASES ( $K_E = 1$ )

In this section, we discuss the evolution of multi-planet systems which are initially fully embedded in a dissipating gas disk with an efficient  $e$  damping. We investigate the effects of gas disk dissipation time (Section 6.1), disk mass (Section 6.2), as well as number of planets (Section 6.3), and study their effects on the final  $a$  and  $e$

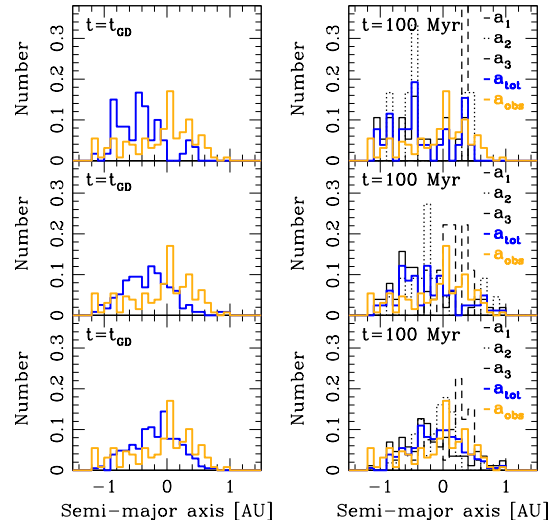


FIG. 3.— Semi-major axis distributions for Set S50, S40, and S30 (from top to bottom) at  $\tau_{GD}$  (left panels), and 100 Myr (right panels). Comparing left panels with right ones, it is apparent that the semimajor axis distributions at  $\tau_{GD}$  are very similar to those at 100 Myr. This implies that planet migration in a gas disk is a dominant process to determine the semimajor axis distribution. On the other hand, the agreement with the observed semimajor axis distribution is not very good, especially for the top two panels. For these sets, planet migration is likely to be too efficient.

distributions.

### 6.1. Effect of gas disk dissipation timescale

#### 6.1.1. Initial Conditions

In this subsection, we focus on the effect of gas disk dissipation timescale on  $a$  and  $e$  distributions. We run three sets of simulations with the same initial disk mass, by changing the gas dissipation time as  $\tau_{GD} = 2, 3,$  and  $4$  Myr (Set tgd2, tgd3, and tgd4, respectively.) Each set consists of 100 three-planet systems, and is evolved for 10 Myr.

The initial disk properties are summarized in Table 1. We obtain the initial disk masses by evolving the MMSN-type disk with  $\Sigma = 10^3(a/\text{AU})^{-1.5} \text{ g cm}^{-2}$ , under the viscosity alpha of  $\alpha = 5 \times 10^{-3}$  (without planets), for a time shown in the second column of Table 1. The corresponding initial disk mass is in the third column. As shown in Table 1, for Set tGD2-tGD4, the initial disk with mass  $M_{disk} = 0.21M_J$  is obtained by evolving the MMSN-type disk for 10 Myr. The initial disk surface mass density is well-approximated by  $\Sigma = 4(a/\text{AU})^{-1} \text{ g cm}^{-2}$ . The gas dissipation timescale for each set is shown in the fourth column. As in the fifth column, we assume  $K_e = 1$ , and hence the efficient eccentricity damping by corotation resonances throughout this section.

#### 6.1.2. Agreement with $a$ and $e$ distributions

The outcomes of the simulations are summarized in Table 2. The collision rates *before*  $\tau_{GD}$  become higher as  $\tau_{GD}$  gets longer (from Set tgd2 to tgd4), while those *after*  $\tau_{GD}$  are low, and about the same for all the sets. This clearly implies that the collision rate with the central star is correlated with the efficiency of planet migration. From Table 2, we see that the rate of ejection of planets is much higher *after*  $\tau_{GD}$  than *before* for all the sets. Therefore, we classify these sets as “late instability” cases.

Fig. 4 compares the observed eccentricity distribution with the simulated results at  $\tau_{GD}$ , and at the end of the simulations, 10 Myr. Two things are immediately apparent from the figure — (1) the distributions at  $\tau_{GD}$  look similar to the ones at 10 Myr for all the sets, and are dominated by planets with  $e \lesssim 0.2$ , and (2) none of the “final” eccentricity distributions for Set tgd2-tgd4 have a good agreement with the observed distribution. Indeed, the K-S tests for the distributions at  $\tau_{GD}$  and at 10 Myr show that we cannot decline the null hypothesis for Set tgd2, and tgd4 at our rejection level ( $P < 0.1$ ), and possibly for Set tgd3 as well, which implies that there is little  $e$  evolution between these two epochs. Also, the K-S tests for the observed  $e$  distribution and the “final”  $e$  distribution (at 10 Myr) indicate that these two distributions are significantly different from each other.

The tendency toward a relatively small eccentricity at  $\tau_{GD}$  agrees well with our expectation from the ejection rates that all the sets are likely to be dynamically stable while a gas disk is around, and therefore planets are expected to be on nearly circular orbits. However, the similarity between the distributions at  $\tau_{GD}$  and 10 Myr, and the difference between the final and observed distributions, indicate that the dynamical instability occurred after the disk removal was too inefficient to reproduce the observed  $e$  distribution for Set tgd2-tgd4.

Fig. 5 shows the corresponding plots for semimajor axis distributions. Again, two things are clear from the figure — (1) the distributions at  $\tau_{GD}$  look similar to the ones at 10 Myr for all the sets, and (2) the agreement with the observed semimajor axis distribution is reasonable for Set tgd2, and tgd3, while for Set tgd4, there are too many planets with small orbital radii. The K-S test for the distributions at  $\tau_{GD}$  and 10 Myr shows that we cannot decline the null hypothesis for all of them, which implies that the semimajor axis distributions are primarily determined while a gas disk is around. On the other hand, the K-S test for the observed and final  $a$  distributions shows that we cannot decline the null hypothesis for Set tgd2 at our chosen rejection level, indicating that the final semi-major axis distribution for Set tgd2 may be consistent with the observations.

It is interesting to apply the definition of dynamically active/inactive systems by JT08 to our results. JT08 proposed that planetary systems could be divided into active, partially active, and inactive systems, depending on (1) the mutual similarity of the final eccentricity distributions, and (2) the degree of evolution. They showed that, when the gas disk dissipates, planetary systems have to be active, or partially active to reproduce the observed  $e$  distribution reasonably well. They also found that the details of the planetary properties at the disk dissipation time are unimportant, or in other words, substantially different ensembles of initial conditions lead to similar final distributions, as long as the systems go through dynamical instability. Similar conclusions are drawn by C08 as well. The first criterion of JT08, the mutual similarity of the final distribution, is a good diagnosis for separating dynamically active systems from the others, while the second criterion is more straightforward, and simply separates systems with little evolution (inactive systems) from the others. They defined that partially active systems are the ones which belong to neither active nor inactive systems. JT08 also found that

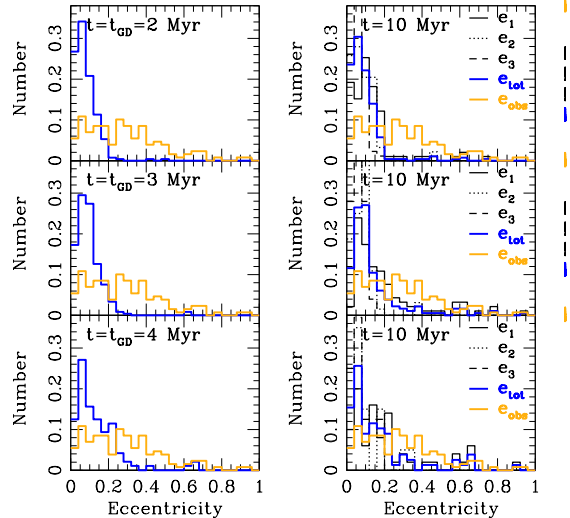


FIG. 4.— Eccentricity distributions for Set tgd2, tgd3, and tgd4 (from top to bottom) at  $\tau_{GD}$  and 10 Myr. Due to the efficient eccentricity damping, there are few planets with eccentricity larger than 0.3 at  $\tau_{GD}$ . On the other hand, there are more planets with high eccentricity at 10 Myr due to planet–planet scattering. None of these sets give a satisfactory match with the observed eccentricity distribution at 10 Myr. However, the agreement improves as the gas dissipation time becomes longer, which may be due to the effect of convergent migration.

such classification is strongly correlated with the median Hill neighbor separation  $\tilde{D}_H$  at  $\tau_{GD}$ . Specifically, they found that planetary systems with  $\tilde{D}_H < 1$  are active,  $4 < \tilde{D}_H < 7$  are partially active, and the only ensemble with  $\tilde{D}_H \simeq 14$  is inactive. This is also indicated by a similar study of C08, who simulated a large number of three-planet systems, and showed that time to dynamical instability becomes longer for larger separation.

Following the definition by JT08, we find that, at least from the disk dissipation time upto the end of our simulations, Set tgd2, and tgd4 stay *inactive*, because the K-S tests for both semimajor axis, and eccentricity distributions imply that there is little evolution between these periods of time. For Set tgd3, the K-S test indicates that the  $e$  distributions at these epochs are significantly different from each other at our rejection level ( $P < 0.1$ ). Therefore we cannot determine its dynamical state from the evolution alone. The median Hill neighbor separations at  $\tau_{GD}$  are  $\tilde{D}_H \simeq 12.2, 13.3,$  and  $14.6$  for Set tgd2, tgd3, and tgd4, respectively. These values are closer to the value obtained for the dynamically inactive system by JT08.

In short, the major indication from these sets of simulations is that planetary systems tend to be dynamically *inactive* (or at most partially active) when a gas disk dissipates, *if* they are initially fully embedded in a gas disk with an efficient eccentricity damping ( $K_e = 1$ ). We further investigate this issue in the next subsection.

## 6.2. Effect of the initial disk mass

### 6.2.1. Initial Conditions

In this subsection, we study the effect of the initial disk mass on  $a$  and  $e$  distributions. Here we use the same set of 100 three-planet systems as the last subsec-

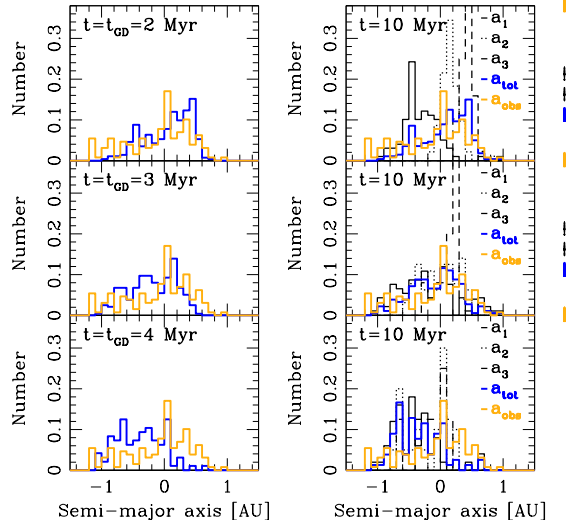


FIG. 5.— Semi-major axis distributions for Set tgd2, tgd3, and tgd4 (from top to bottom) at  $\tau_{GD}$ , and 10 Myr. Again, we find that there is little  $a$  evolution between these periods of time. Top panel (Set tgd2) gives a good agreement with the observations, while bottom two panels, especially Set tgd4, overproduce close-in planets, indicating too efficient migration.

TABLE 1  
INITIAL DISK CONDITIONS

Set No.	$\tau_{disk}$ [Myr]	$M_{disk}$ [ $M_J$ ]	$\tau_{GD}$ [Myr]	$K_e$
S50	N/A	0.45	2-5	1
S40	N/A	0.36	2-5	1
S30	N/A	0.27	2-5	1
tgd2	10	0.21	2	1
tgd3	10	0.21	3	1
tgd4	10	0.21	4	1
t7	7	0.71	2-5	1
t9	9	0.32	2-5	1
t10	10	0.21	2-5	1
t11	11	0.14	2-5	1
t13	13	0.06	2-5	1
t10p5	10	0.21	2-5	1
t10p7	10	0.21	2-5	1
t10ke0	10	0.21	2-5	0
t10ke05	10	0.21	2-5	0.5
t8cr	8	0.47	2-5	CR
t9cr	9	0.32	2-5	CR
t10cr	10	0.21	2-5	CR
t11cr	11	0.14	2-5	CR
t7cr2	7	0.71	1-3	CR
t8cr2	8	0.47	1-3	CR
t9cr2	9	0.32	1-3	CR
t10cr2	10	0.21	1-3	CR

NOTE. — Initial conditions for each set of 100 runs. Column 2 shows the age of initial disks, which is obtained by evolving a MMSN-type disk under  $\alpha = 2 \times 10^{-3}$ . Column 3 lists the corresponding initial disk mass. Column 4 is the gas disk dissipation timescale measured from the start of the simulation, and the disk is removed exponentially once this time is reached. The dissipation timescale  $\tau_{GD} = 2 - 5$  Myr means that  $\tau_{GD}$  is randomly chosen between these values. Column 5 shows the eccentricity damping factor  $K_e$ , where 1 is full damping, 0 is no-damping, and CR means that the saturation of corotation resonances is taken into account as explained in Section 3.2.

tion, and choose the gas dissipation time randomly from 2 – 5 Myr for each of them. We run 5 different sets of 100 systems for 100 Myr by changing the initial disk mass systematically from  $0.71 M_J$  to  $0.06 M_J$ . Each initial disk is generated by evolving the MMSN-type disk with  $\Sigma = 10^3 (a/AU)^{-3/2} g cm^{-2}$  for 7, 9, 10, 11, and 13 Myr (hereafter Set t7, t9, t10, t11, and t13, respectively.) These initial conditions are shown in Table 1.

### 6.2.2. Agreement with $a$ and $e$ distributions

Table 2 summarizes the results of the numerical simulations for these sets. Set t7, t9, t10, and t11 show a similar *total* number of ejected planets. However, the timing of ejections are markedly different.

For the most massive disk case (Set t7), the ejections mainly occur *while* a gas disk is still around ( $\tau_{dyn} < \tau_{GD}$ , i.e. “early instability” case), and for Set t9, the ejections occur at similar rates both before and after  $\tau_{GD}$  (i.e. “multiple instability” case). On the other hand, for less massive disks (Set t10 and t11), the ejections primarily occur *after* the gas disk is gone ( $\tau_{GD} < \tau_{dyn}$ , i.e. “late instability” cases), while for the least massive disk (Set t13), there are few numbers of collisions and ejections, indicating that there is little evolution. Below, we mainly focus on the results of Set t9, t10, and t11, since Set t7 is left with too few planets at 100 Myr to do a statistical study, and Set t13 did not evolve much.

In Fig. 6, the observed eccentricity distribution is compared with our numerical results at  $\tau_{GD}$ , and 100 Myr, for Set t9, t10, and t11. From the figure, it appears (1) the “multiple instability” case (Set t9) has some highly eccentric planets at  $\tau_{GD}$ , while in “late instability” cases (Set t10, and t11), most planets are  $e \lesssim 0.2$ , (2) there seems to be  $e$  evolution between  $\tau_{GD}$  and 100 Myr, but (3) none of these sets look similar to the observed  $e$  distribution at 100 Myr.

For “late instability” cases, the K-S tests show that the  $e$  distributions at  $\tau_{GD}$  and 100 Myr are different from each other at our rejection level, indicating that there was a significant  $e$  evolution between these periods of time. However, the K-S tests for the final and observed  $e$  distributions show that these distributions are significantly different from each other, implying that the dynamical evolution for these sets was not efficient enough to reproduce the observed distribution.

For “multiple instability” case, the K-S test shows that we cannot decline the null hypothesis for the  $e$  distributions at  $\tau_{GD}$  and 100 Myr. This implies that there was little evolution between these two epochs, although there seems to be non-negligible change in  $e$  distribution in Fig. 6. The K-S test confirms that the final  $e$  distribution is significantly different from the observed one.

In Fig. 7, we show the corresponding plots for semi-major axis. Here, we find (1) there seems to be little  $a$  evolution between  $\tau_{GD}$  and 100 Myr, and (2) the agreement with the observed distribution becomes better from Set t9 to t11. The K-S tests for the  $a$  distributions at  $\tau_{GD}$  and 100 Myr show that we cannot rule out the null hypothesis for all of these sets at more than 10% level, which again indicates that the  $a$  distribution is primarily determined while planets are still embedded in a gas disk. The K-S tests also show that, for Set t11, we cannot rule out the null hypothesis for the final and observed  $a$  distributions, which implies that the final distribution of

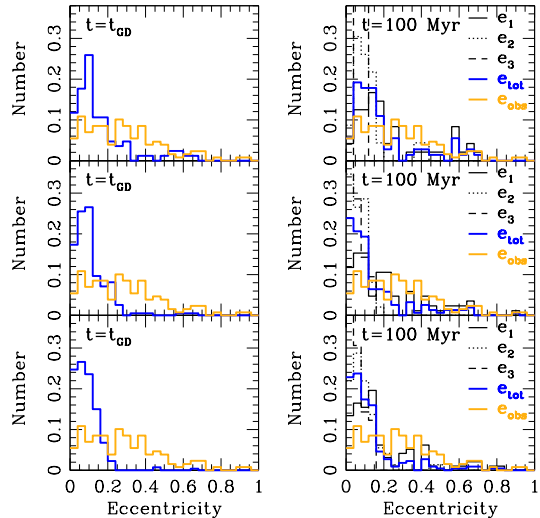


FIG. 6.— Eccentricity distributions for Set t9, t10, and t11 (from top to bottom) at  $\tau_{GD}$  and 100 Myr. Due to the efficient eccentricity damping, there are few planets with eccentricity larger than 0.3 at  $\tau_{GD}$ , while there are more planets with high eccentricity at 100 Myr due to planet–planet scattering. None of these sets give a satisfactory match with the observed eccentricity distribution at 100 Myr. The agreement improves as the initial disk mass increases.

Set t11 may be consistent with the observed one.

In summary, we find that a “late instability” case, Set t11, can reproduce the observed  $a$  distribution reasonably well, but the dynamical instability occurred after  $\tau_{GD}$  is not efficient enough to reproduce the observed  $e$  distribution. The median Hill neighbor separations at  $\tau_{GD}$  are  $\bar{D}_H \simeq 14.7, 12.6, 11.4,$  and  $10.5$  for Set t9, t10, t11, and t13, respectively. These values are closer to the value obtained for the inactive system by JT08. In short, we find that three-planet systems, which are initially fully embedded in a gas disk with an efficient eccentricity damping ( $K_e = 1$ ), stay overall dynamically inactive after the gas disk dissipation until the end of our simulations.

### 6.3. Effect of Number of Planets

#### 6.3.1. Initial Conditions

In this subsection, we investigate the effect of numbers of planets on  $a$  and  $e$  distributions. Specifically, we study the evolution of five- and seven-planet systems which are initially fully embedded in the identical gas disk to Set t10. We call sets of five- and seven-planet systems as Set t10p5, and t10p7, respectively. The initial planetary properties are determined in a similar manner to three-planet systems, and we simulate 100 planetary systems each for 100 Myr.

#### 6.3.2. Agreement with $a$ and $e$ distributions

From Table 2, we find that both sets are “late instability” cases, since their ejection rates are much higher after  $\tau_{GD}$ . Comparing these two sets with a three-planet case (Set t10), we find that the ejection rates dramatically increase with the number of planets. The ejection rates *before*  $\tau_{GD}$  are 3, 6.8 and 6.4% for three-, five- and seven-planet systems, respectively, while those *after*  $\tau_{GD}$  are 23.1, 41.9 and 74.9%.

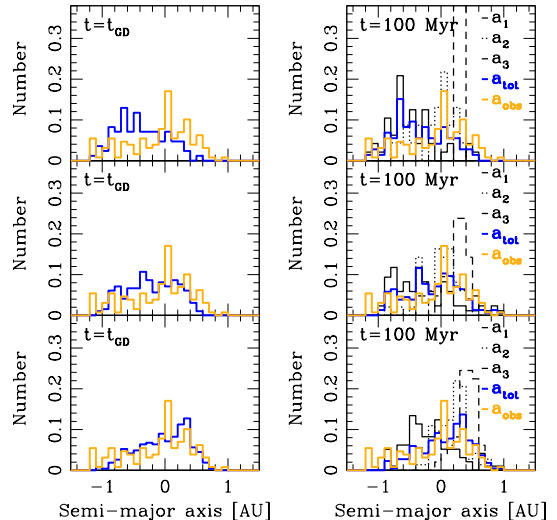


FIG. 7.— Semi-major axis distributions for Set t9, t10, and t11 (from top to bottom) at  $\tau_{GD}$ , and 100 Myr. Again, there is little  $a$  evolution between these periods of time. Bottom panel (Set td11) gives a good agreement with the observations, while top two panels (Set td9 and td10) overproduce close-in planets.

On the other hand, we don’t find any significant dependence on the number of planets per system for the collision rates with the central star, which are 29, 24.4, and 24.1% before  $\tau_{GD}$ , and 2.7, 4.8, and 5.0% after that for Set t10, t10p5, and t10p7, respectively. This coincides with the expectation that the collision rates are mainly determined by planet migration, and thus by the strength of the disk–planet interactions, rather than the planet–planet interactions. The merger rates also show a similar value, although the rate slightly increases with the number of planets per system.

In Fig. 8, we show the evolution of eccentricity distributions for five- and seven-planet systems (top, and bottom panels, respectively), compared with the observed distribution at  $\tau_{GD}$  and 100 Myr. We find that (1) as expected from the ejection rates, most planets have  $e \lesssim 0.2$  at  $\tau_{GD}$ , and (2) despite the high ejection rates after  $\tau_{GD}$ , neither final distributions agree well with the observed  $e$  distribution.

The K-S tests show that the  $e$  distributions at  $\tau_{GD}$  and 100 Myr are significantly different from each other, implying that there was non-negligible  $e$  evolution between these two periods of time. However, as the K-S tests for the final and observed distributions show, the dynamical instability occurred after  $\tau_{GD}$  turned out to be not efficient enough to reproduce the observed distribution. Note however, that the agreement is better if we focus on very high eccentricity planets ( $e > 0.4$ ). It appears that these systems overproduce planets with a relatively low eccentricity ( $e \lesssim 0.2$ ), while they *underproduce* planets with intermediate eccentricity ( $0.2 < e < 0.4$ ).

In Fig. 9, we show the corresponding plots for semi-major axis. We find (1) as expected from the high ejection rates after the disk dissipation, there is a significant  $a$  evolution between  $\tau_{GD}$  and 100 Myr, and (2) final  $a$  distribution of Set t10p5 agrees well with the observed distribution within the observation limit. When we limit ourselves to the planets between 0.2 and 6 AU, we find that the final  $a$  distribution of Set t10p5 may be consis-

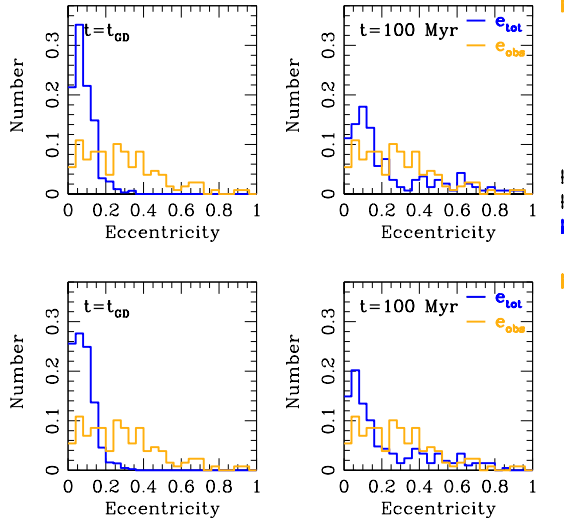


FIG. 8.— Eccentricity distributions for five- and seven-planet systems (top, and bottom panels, respectively) at  $\tau_{GD}$  and 100 Myr. In both cases, the results look very similar to three-planet systems. There are few planets with eccentricity larger than 0.3 at  $\tau_{GD}$  due to the efficient eccentricity damping in the disk, while more planets with high eccentricity are found at 100 Myr due to planet–planet scattering. Neither of these sets give a satisfactory match with the observed eccentricity distribution at 100 Myr, despite high ejection rates.

tent with the observed one.

In summary, we find that more planetary systems become dynamically unstable (i.e. ejection rates increase) after the disk dissipation as we increase the number of planets per system. However, we do not find a significant improvement in the agreement between the simulations and the observations. Our results indicate that the dynamical instability after  $\tau_{GD}$  can reproduce the higher-end ( $e > 0.4$ ) of the  $e$  distributions, while there is a deficit of planets with an intermediate eccentricity ( $0.2 < e < 0.4$ ). Just to complete our summary, we note that their median Hill neighbor separations at  $\tau_{GD}$  are rather large and  $\bar{D}_H \simeq 10.6$ , and 11.8 for five-, and seven-planet systems, respectively.

## 7. INEFFICIENT ECCENTRICITY DAMPING CASES ( $K_e \neq 1$ )

In this section, we investigate the evolution of multi-planet systems in a disk with less efficient eccentricity damping compared to the previous sections. First, we investigate the cases with constant  $K_e$  in Section 7.1, and then we show the cases where we take account of the saturation effect of corotation resonances in Section 7.2. Finally, we briefly discuss planets in mean motion resonances in Section 7.3.

### 7.1. Effect of the damping factor $K_e$

#### 7.1.1. Initial Conditions

In this subsection, we show two other cases with constant  $K_e$  values —  $K_e = 0$ , and 0.5, by assuming otherwise the same initial conditions as Set t10 (where  $K_e = 1$ .) We call these sets of 100 three-planet systems as Set t10ke0, and t10ke05, respectively.

#### 7.1.2. Agreement with $a$ and $e$ distributions

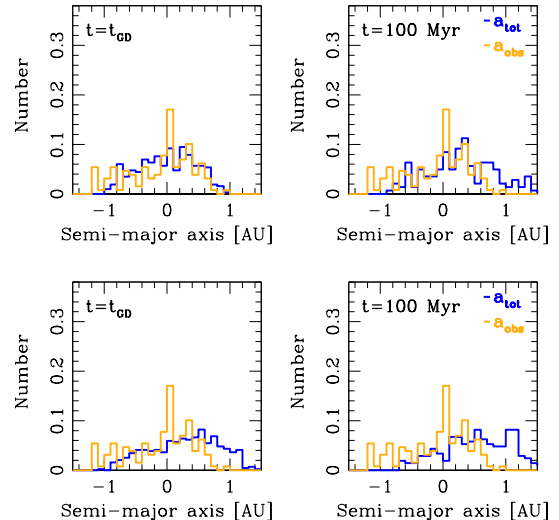


FIG. 9.— Semi-major axis distributions for five- and seven-planet systems (top, and bottom panels, respectively) at  $\tau_{GD}$ , and 100 Myr. As indicated by high ejection rates, both distributions are broader than three-planet systems. The final distribution for Set t10p5 gives a good agreement with observations between 0.2 and 6 AU.

From Table 2, we find that the collision rates before  $\tau_{GD}$  decrease with  $K_e$ , while the corresponding ejection and merger rates increase. Therefore, with weaker  $e$  damping, more planetary systems become dynamically unstable before the gas disk dissipation. We classify Set t10ke0 and t10ke05 as an “early instability”, and “late instability” case, respectively, based on the ejection rates before and after  $\tau_{GD}$ .

Fig. 10 compares the observed and simulated  $e$  distributions at  $\tau_{GD}$  and 100 Myr for Set t10ke0, t10ke05, and t10. We find (1) as expected from the ejection rates, Set t10ke0 has many high  $e$  planets at  $\tau_{GD}$ , while the others mostly have planets with  $e \lesssim 0.2$ , and (2) eccentricities have a broader distribution for smaller  $K_e$ . The K-S test for Set t10ke0 shows that we cannot rule out the null hypothesis for the observed and final distributions, which indicates that the set may be consistent with the observed  $e$  distribution.

Fig. 11 shows the corresponding plots for semi-major axis. For  $a$  distributions, we do not find as large dependence on  $K_e$  as eccentricities. However, it is apparent that there are less planets on short-orbital periods for smaller  $K_e$ , which implies that planet–planet interactions play a more important role in determining the  $a$  distributions for less efficient damping cases. The K-S test for Set t10ke0 shows that we cannot decline the null hypothesis for observed and final distributions, which indicates that the set may also be consistent with the observed  $a$  distribution.

In summary, we find that both  $a$  and  $e$  distributions can be reproduced well in a dissipating gas disk, if there is no  $e$  damping (Set t10ke0). Obviously, this is not a realistic case, since it’s unlikely that we can neglect the  $e$  damping effect due to disk–planet interactions completely. In the next subsection, we further investigate this by adopting an inefficient  $e$ -damping prescription.

### 7.2. Effect of the Initial Disk Mass and $\tau_{GD}$

#### 7.2.1. Initial Conditions

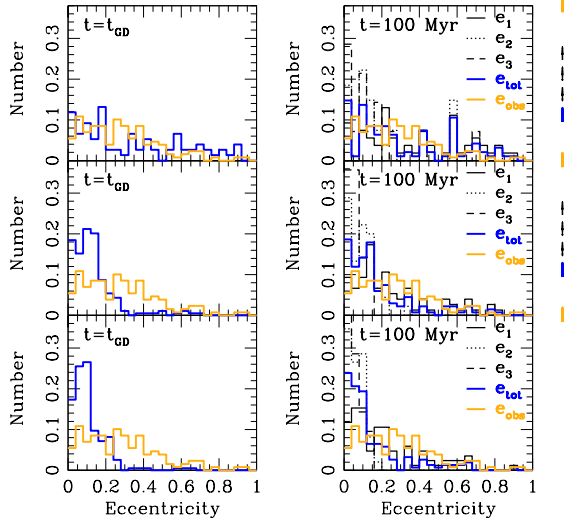


FIG. 10.— Eccentricity distributions for Set t10Ke0, t10Ke05, and t10 (from top to bottom) at  $\tau_{GD}$  and 100 Myr. As the  $K_e$  decreases, the  $e$  distribution becomes broader. When there is no eccentricity damping (Set t10ke0), the planetary systems become dynamically unstable while they are still in the gas disk. While for more efficient  $e$ -damping cases (Set t10ke05, and t10), the planetary systems don’t have many planets with  $e \gtrsim 0.3$  at  $\tau_{GD}$ . The final distribution for Set t10ke0 gives a good agreement with the observations.

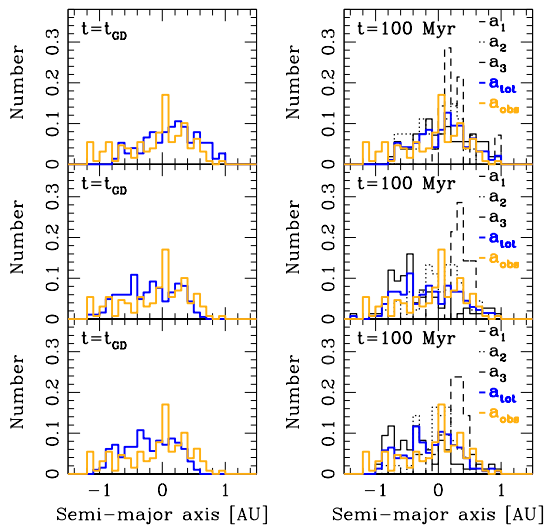


FIG. 11.— Semi-major axis distributions for Set t10Ke0, t10Ke05, and t10 (from top to bottom) at  $\tau_{GD}$ , and 100 Myr. The peak of a distribution occurs at larger  $a$  for smaller  $K_e$ , which indicates planet-planet scattering plays an important role in determining the distribution for such cases. Set t10ke0 gives a good agreement with the observations.

In this subsection, we study the effects of eccentricity damping by taking account of the saturation of corotation resonances (see Section 3.2). We focus on the effects of two parameters — disk mass, and gas dissipation timescale.

We take the same 100 three-planet systems as before, and choose two different ranges of the disk dissipation time 2 – 5 Myr, and 1 – 3 Myr.

For  $\tau_{GD} = 2 - 5$  Myr, we run four sets of simulations with initial disks obtained by evolving the MMSN-type disk for 8, 9, 10, and 11 Myr without planets. We refer to

these sets as Set t8cr, t9cr, t10cr, and t11cr, respectively. Similarly, for  $\tau_{GD} = 1 - 3$  Myr, we run other four sets of simulations with initial disks obtained by evolving the MMSN-type disk for 7, 8, 9, and 10 Myr without planets. These sets are called Set t7cr2, t8cr2, t9cr2, and t10cr2, respectively.

All of these simulations are run for 100 Myr. Again, the initial disk properties are summarized in Table 1.

### 7.2.2. Agreement with $a$ and $e$ distributions for $\tau_{GD} = 2 - 5$ Myr

Here, we discuss the results for Set t8cr-t11cr. From Table 2, we find that, for all of these four sets, the ejection rates are much higher before  $\tau_{GD}$  (“early instability” cases), while the collisions are almost negligible compared to the ejections. This is a similar trend to Set t10ke0. Since the ejection rate after  $\tau_{GD}$  reaches 100% for Set t8cr (which means that there are two multiple planetary systems at  $\tau_{GD}$  and both of them lost a planet through ejection), we can expect that the ejection rates saturate for the set. Below, we limit our discussion to the other three sets.

Set t9cr-t11cr can be directly compared to the results of Set t9-t11 in Section 6.3, where  $K_e = 1$ . It is apparent that the former sets are more dynamically active than the latter ones. Even the most inactive Set t11 ejects many planets when we take account of the saturation of corotation torques (Set t11cr).

In Fig. 12, we compare the simulated and observed  $e$  distributions at  $\tau_{GD}$  and 100 Myr for these sets. It is apparent that (1) all of these sets look similar to a zero  $e$ -damping case in the last subsection, rather than the more efficient damping cases, and (2) all of them have overall a similar trend to the observed  $e$  distribution. In fact, we cannot reject the null hypothesis for the observed and final  $e$  distributions for Set t9cr, and t11cr, which implies that these  $e$  distributions may be consistent with the observed distribution. The K-S tests also show that the null hypothesis for distributions at  $\tau_{GD}$  and 100 Myr cannot be ruled out for any of these sets (including Set t8cr), which implies that there is little  $e$  evolution between these epochs.

In Fig. 13, we show the corresponding plots for semi-major axis. Comparing with Fig. 7 for Set t9-t11, we find that the peaks of the distributions tend to occur at larger  $a$  for the same initial disk mass, which indicates that planet-planet interactions significantly contribute to the orbital evolution of planets for Set t9cr-t11cr. Also, the peaks move outward with the decrease in the initial disk mass, which indicates less efficient migration due to planet-disk interaction for less massive disks. The K-S tests for observed and final distributions show that we cannot rule out the null hypothesis for Set t10cr, and t11cr.

In summary, we find that, when we take account of the saturation effect of corotation torques, we can reproduce both  $a$  and  $e$  distributions simultaneously (Set t11cr). These results look similar to the case with zero  $e$  damping, rather than conventional, more efficient damping. The K-S tests show that neither  $a$  nor  $e$  distributions change significantly after the gas disk dissipation, which implies that the final  $a$ - $e$  distributions are primarily determined while a gas disk is around, not after the disk dissipation.

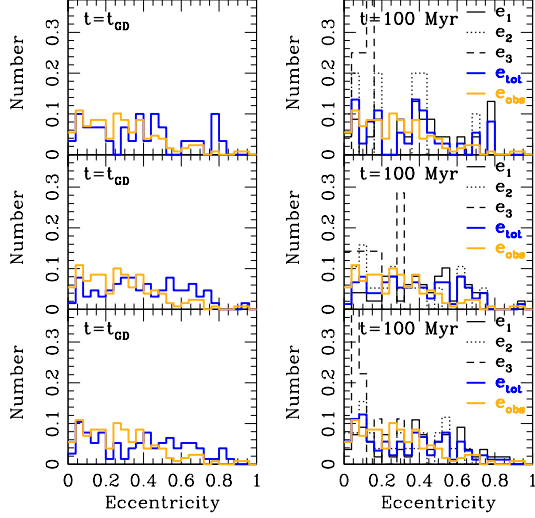


FIG. 12.— Eccentricity distributions for Set t9cr, t10cr, and t11cr (from top to bottom) at  $\tau_{GD}$  and 100 Myr. Inefficient  $e$  damping leads to earlier occurrence of dynamical instability. Set t9cr, and t11cr give a good agreement with the observations.

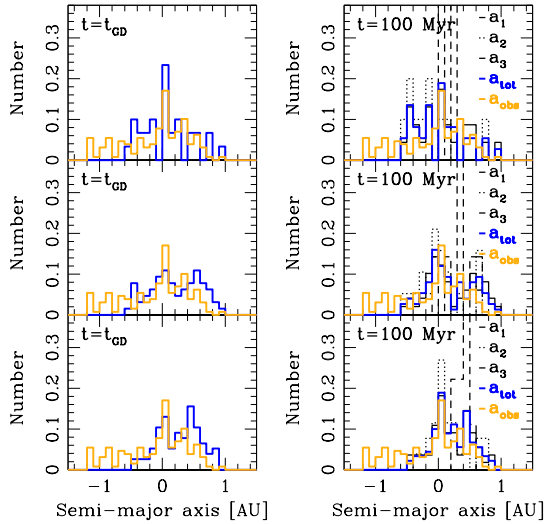


FIG. 13.— Semi-major axis distributions for Set t9cr, t10cr, and t11cr (from top to bottom) at  $\tau_{GD}$ , and 100 Myr. There is little evolution between these periods of time. Set t10cr, and t11cr give a good agreement with the observations.

### 7.2.3. Agreement with $a$ and $e$ distributions for $\tau_{GD} = 1 - 3$ Myr

Here, we discuss the results for Set t7cr2-t10cr2. From Table 2, we find that, for all of these four sets, the ejection rates are higher before  $\tau_{GD}$  (“early instability” cases), and the collision rates are very small, as in the last subsection.

Comparing Set t8cr2-t10cr2 with Set t8cr-t10cr in the last subsection, we find that the ejection rates before  $\tau_{GD}$  are much smaller due to the shorter gas dissipation time.

In Fig. 14, we compare the simulated and observed  $e$  distributions at  $\tau_{GD}$  and 100 Myr for Set t7cr2-t9cr2. Similar to the results in the last section, we find these  $e$  distributions are much broader than the efficient  $e$ -damping cases, and similar to the observed distribution. In fact, for our rejection level, we cannot decline the

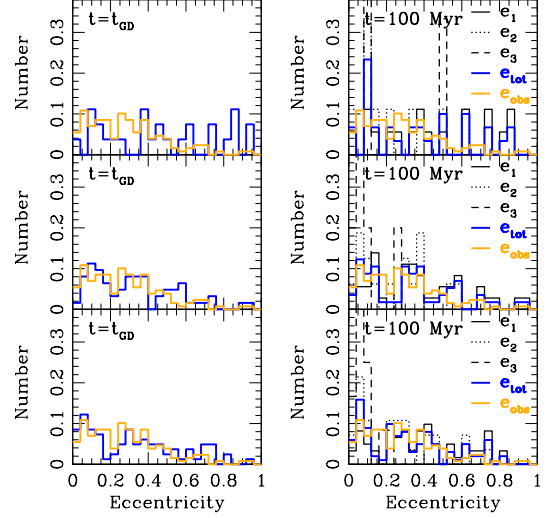


FIG. 14.— Eccentricity distributions for Set t7cr2, t8cr2, and t9cr2 (from top to bottom) at  $\tau_{GD}$  and 100 Myr. The overall trend looks similar to Fig. 12. All of these sets give a good agreement with the observations.

null hypothesis for any of these sets, including Set t10cr2 which is not shown here. This implies that all of these sets lead to the  $e$  distributions which may be consistent with the observations.

In Fig. 15, we show the corresponding plots for semi-major axis. Again, we find that the peaks in the distribution moves outward with the decrease in the initial disk mass. The K-S tests show that, for observed and final distributions, the null hypothesis cannot be ruled out for any of these sets, but Set t10cr2.

Therefore, it appears that Set t7cr2-t9cr2 may be consistent with both the observed  $a$  and  $e$  distributions. Fig. 16 is the final  $a$ - $e$  scattered plot for Set t7cr2-t9cr2 (blue circles), compared with the observed plot (orange circles). We find that these two scattered plots cover a similar region of parameter space within the numerical and observational limits. Also plotted are the orbital properties of discarded planets just before they are removed from the simulations via ejection, collision, or merger. These planets also follow the trend of the observed scattered plot. The 2D K-S test between 0.2 and 6 AU for observed and final distributions shows that we cannot reject the null hypothesis for these two distributions at less than 2.5% significance level, which implies that these two distributions are likely to be consistent with each other.

In summary, we find that the observed  $a$  and  $e$  distributions can be simultaneously reproduced if we assume that planets are originally fully embedded in a gas disk with inefficient  $e$  damping. All of our “successful” cases suggest that major dynamical instability events should occur *before* the gas disk dissipation, rather than after that (as suggested by N-body simulations without a gas disk).

### 7.3. Mean Motion Resonances

In the previous subsections, we find that the  $a$  and  $e$  distributions of some of our sets may be consistent with the observed ones (Set t7cr2, t8cr2, t9cr2, and t11cr). It is interesting to investigate whether any of these systems are on mean motion resonances (MMRs). Although it’s

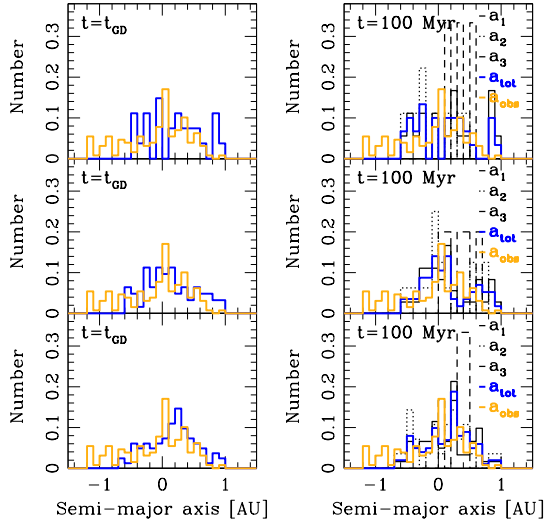


FIG. 15. — Semi-major axis distributions for Set t7cr2, t8cr2, and t9cr2 (from top to bottom) at  $\tau_{GD}$ , and 100 Myr. The overall trend looks similar to Fig. 13. All of these sets give a good agreement with the observations.

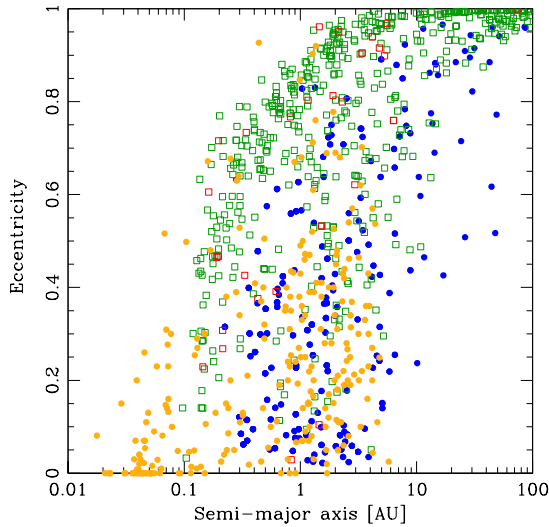


FIG. 16. — The  $a$ - $e$  scattered plot for Set t7cr2, t8cr2, and t9cr2 at 100 Myr (blue circles), compared with the observed distribution (orange circles). Also plotted are the final orbital properties for ejected, collided, and merged planets (green, red, and black squares, respectively.) The simulated planets cover a similar parameter space to the observed ones.

still too early to derive any statistical trend, some of the observed systems are known to be in MMRs.

At the end of the simulations, Set t7cr2, t8cr2, t9cr2, and t11cr have 4/21, 9/48, 19/72, and 17/69 multi-planet systems, respectively. For each of these systems, we evaluate whether they are in a particular resonance by using the following resonance variable (Murray & Dermott 1999):

$$\varphi = j_1 \lambda_o + j_2 \lambda_i + j_3 \varpi_o + j_4 \varpi_i, \quad (7)$$

where  $\lambda$  and  $\varpi$  are the mean longitude and longitude of pericenter, respectively, and the subscripts  $i$  and  $o$  indicate inner and outer planets. Here, we focus on near coplanar cases, and thus neglect the terms regarding the longitude of ascending node. When planets are in  $p+q : p$

MMR, we can define  $(j_1, j_2, j_3, j_4) = (p+q, -p, -q, 0)$ , or  $(p+q, -p, 0, -q)$ .

We follow first- to third-order resonances (2:1, 3:2, 3:1, 5:3, 4:1, 5:2), as well as some higher order resonances (5:1, 7:3, 6:1, 7:2, 7:1, 8:1, 9:2, 9:1, 11:3). We find that three systems are clearly in MMRs for Set t11cr, out of which two are in 2:1, and the other is in 4:1 MMR. We do not find any resonant systems for the other sets, although some systems have period ratios indicating MMRs. Naively speaking, these results indicate that about 6.1% of planetary systems are in MMRs. This is somewhat consistent with recent N-body studies by Raymond et al. (2008). Studying dynamical instabilities of three-planet systems, they found that planet-planet scattering could generate planets in both low- and high-order MMRs, and that roughly 5 – 10% of dynamically unstable systems ended up being in MMRs.

## 8. SUMMARY

We have studied multiple-planet systems with a dissipating gas disk by means of the hybrid code which combines the N-body symplectic integrator SyMBA, and a one-dimensional gas disk evolution code. The main goal for this study is to investigate different plausible scenarios and understand how different initial conditions affect the final distributions of observable orbital properties. Specifically, we have considered three different kinds of initial setups — (1) planets in the inner cavity of a disk, (2) planets fully embedded in a disk with an efficient  $e$  damping, and (3) planets fully embedded in a disk with less efficient damping.

In Section 5, we have studied the first case for three-planet systems. For such a setup, the surrounding gas disks help efficient convergent migration between planets, which tends to lead to dynamical instability, and excite planetary eccentricities. The instability tends to set in earlier for planetary systems in more massive disks. Our results suggest that this kind of setups can reproduce the observed  $e$  distribution, while they are likely to overproduce planets with small semi-major axes. We note, however, that our simulations don't take account of planet formation. For example, multiple planet formation simulations like TMR08 suggest that the disks' cavities repeatedly get "reset" when later generations of planets form, i.e the outermost planet becomes the second-outermost, and so forth. This may play an important role in getting a more favorable semimajor axis distribution out of the cavity scenario.

In Section 6, we have investigated the second case, by focusing on the effects of gas dissipation time (Section 6.1), initial disk mass (Section 6.2), and number of planets per system (Section 6.3). Collision rates become higher, and thus planet migration is more efficient for more massive disks with longer  $\tau_{GD}$ , while the number of planets per system does not affect the collision rates significantly. On the other hand, ejection rates increase with the number of planets, while they are not strongly affected by the disk properties unless the disk mass is very small and thus the disk cannot help convergent migration.

Our major findings for an efficient  $e$  damping case are (1) gas disks indeed help reproducing the observed semi-major axis distribution, (2) gas disks tend to overly damp the eccentricity of planets, and (3) planetary systems

tend to be dynamically *inactive* when they emerge out of the gas disks.

In Section 7, we investigated the third case, by focusing on the effects of the damping factor  $K_e$  (Section 7.1), as well as the initial disk mass and  $\tau_{GD}$  (Section 7.2). Our results suggest that inefficient  $e$  damping may be necessary to reproduce observed  $a$  and  $e$  distributions simultaneously, and that in such a case, the dynamical instability tends to set in *before* the gas disk dissipation. Therefore, it is likely that the final orbital distributions are primarily determined as the gas disk dissipates, rather than after the disk dissipation, as suggested by previous N-body simulations.

In the following, we list several uncertainties in our investigations about the origins of the observed properties of extrasolar planetary systems.

First of all, the initial conditions for this kind of simulations are highly uncertain. For most of our systems, we assume that nearly fully-grown giant planets are embedded in a gas disk, while in reality, planets would start opening gaps as they grow. However, the planets in our simulations open gaps in a time on the order of the orbital periods (i.e. less than several tens of years), which are shorter than, or at most comparable to, both the dynamical, and migration timescales. Therefore, we don't expect a huge difference in the outcome due to this approximation.

Also, our choice of the initial planetary properties like mass, and semimajor axis are rather arbitrary, and we adopt the initial conditions that are motivated by the core accretion scenario. To better approximate the initial conditions, we could perform planet formation simulations as in TMR08. However, such simulations are computationally very expensive for performing statistical studies.

Secondly, the disk-planet interactions in our disk models do not include the effects of corotation resonances directly. Since corotation torques are sensitive to sharp gradients in the surface mass density, they may have a significant effect on the planets simulated here, which are massive enough to open a gap in the disk. However, at the same time, the corotation torques tend to saturate if the gap is cleanly open (Goldreich & Sari 2003). Since the corotation torques tend to accelerate the inward planet migration (Masset & Papaloizou 2003), as well as damp the eccentricity against the Lindblad torques, these facts together imply that we are likely to underestimate (1) planet migration rates for intermediate-mass (Saturn-like) planets, which do not open a clean gap, and (2) eccentricity excitation rate for massive planets, which open a clean gap. Therefore, our planet migration, as well as

eccentricity excitation rates are really lower limits.

In our simulations, the eccentricity damping effect is calculated indirectly from Eq. 3. The choice of coefficient  $K_e$  is arbitrary. We simply assume that  $K_e = 1$  corresponds to the maximum eccentricity damping, and normalize the effect of the saturation of corotation torques accordingly (see Eq. 4). Hence, the effectiveness of eccentricity damping considered here is strictly in a relative sense. To better evaluate its effect, one would have to perform full hydrodynamic simulations. Although we encourage such studies, they are unfortunately out of the scope of this work.

Finally, our gas disk is removed exponentially once the randomly selected disk dissipation time is reached. Although such a disk removal is included to mimic the effect of photoevaporation, we did not model its physics directly. This is because the photoevaporation rate is difficult to estimate accurately, due to its sensitivity to the stellar flux, which in turn depends on the disk accretion rate, as well as the stellar environment (Matsuyama et al. 2003).

In summary, through our simulations, we find the following:

(1) The initial conditions of the N-body simulations without a gas disk, where planets are closely separated so that they are dynamically “active”, are difficult to achieve. In our simulations, most systems turn out to be dynamically inactive, or partially active at most, when the gas disk is gone.

(2) Planet migration in a gas disk mostly determines the final semimajor axis distributions. We find that the general trend of semimajor axis distributions is similar at the gas disk dissipation time, and at the end of the simulations.

(3) To reproduce both semimajor axis and eccentricity distributions of extrasolar planets simultaneously, the eccentricity damping due to disk-planet interactions may need to be inefficient, possibly due to the saturation of corotation torques.

(4) For four sets which can reproduce the  $a$  and  $e$  distributions simultaneously, we find that about 6.1% of multi-planet systems stay on MMRs at the end of the simulations.

This work was supported by NSF Grant AST-0507727 (to F. A. R.) and by a Spitzer Theory grant, as well as a grant from Natural Sciences and Engineering Research Council of Canada (to E. W. T.). S. M. extends a sincere thank you to Ralph Pudritz for making SHARCNET available for many of the simulations shown in this work.

## REFERENCES

- Adams, F. C. & Laughlin, G. 2003, *Icarus*, 163, 290  
 Alexander, R. D., Clarke, C. J., & Pringle, J. E. 2006, *MNRAS*, 369, 229  
 Bryden, G., Lin, D. N. C., & Ida, S. 2000, *ApJ*, 544, 481  
 Chatterjee, S., Ford, E. B., Matsumura, S., & Rasio, F. A. 2008, *ApJ*, 686, 580  
 D'Angelo, G., Kley, W., & Henning, T. 2003, *ApJ*, 586, 540  
 D'Angelo, G., Lubow, S. H., & Bate, M. R. 2006, *ApJ*, 652, 1698  
 Duncan, M. J., Levison, H. F., & Lee, M. H. 1998, *AJ*, 116, 2067  
 Ford, E. B. & Rasio, F. A. 2007, *ArXiv Astrophysics e-prints*  
 Goldreich, P. & Sari, R. 2003, *ApJ*, 585, 1024  
 Hillenbrand, L. A. 2005, review article in “A Decade of Discovery”, *astro-ph/0511083*  
 Jurić, M. & Tremaine, S. 2008, *ApJ*, 686, 603  
 Kokubo, E. & Ida, S. 2002, *ApJ*, 581, 666  
 Kominami, J. & Ida, S. 2004, *Icarus*, 167, 231  
 Lewis, J. S. 1974, *Science*, 186, 440  
 Lin, D. N. C. & Papaloizou, J. 1986, *ApJ*, 307, 395  
 Lodders, K. 2004, *ApJ*, 611, 587  
 Masset, F. S. & Papaloizou, J. C. B. 2003, *ApJ*, 588, 494  
 Matsumura, S., Pudritz, R. E., & Thommes, E. W. 2009, *ApJ*, 691, 1764  
 Matsuyama, I., Johnstone, D., & Hartmann, L. 2003, *ApJ*, 582, 893  
 Menou, K. & Goodman, J. 2004, *ApJ*, 606, 520  
 Moorhead, A. V. & Adams, F. C. 2005, *Icarus*, 178, 517

TABLE 2  
EJECTED, COLLIDED, AND MERGED PLANETS

Set No.	Ejections			Collisions			Mergers		
	Before $\tau_{GD}$	After $\tau_{GD}$	Total	Before $\tau_{GD}$	After $\tau_{GD}$	Total	Before $\tau_{GD}$	After $\tau_{GD}$	Total
S50	65 (21.7)	13 (29.5)	78	155 (51.7)	4 (9.1)	159	20 (6.7)	0 (0)	20
S40	38 (12.7)	23 (24.5)	61	113 (37.7)	5 (5.3)	118	24 (8)	0 (0)	24
S30	15 (5)	55 (28.4)	70	42 (14)	4 (2.1)	46	35 (11.7)	2 (1.0)	37
tgd2	0 (0)	37 (13.0)	37	2 (0.7)	1 (0.4)	3	14 (4.7)	0 (0)	14
tgd3	12 (4)	67 (29.0)	79	37 (12.3)	8 (3.5)	45	14 (4.7)	0 (0)	14
tgd4	26 (8.7)	22 (19.3)	48	119 (39.7)	2 (1.8)	121	14 (4.7)	0 (0)	14
t7	40 (13.3)	0 (0)	40	248 (82.7)	0 (0)	248	10 (3.3)	0 (0)	10
t9	45 (15)	10 (16.1)	55	159 (53)	3 (4.8)	162	10 (3.3)	0 (0)	10
t10	9 (3)	43 (23.1)	52	87 (29)	5 (2.7)	92	7 (2.3)	0 (0)	7
t11	5 (1.7)	53 (20)	58	19 (6.3)	5 (1.9)	24	9 (3)	0 (0)	9
t13	2 (0.7)	4 (1.7)	6	0 (0)	1 (0.4)	1	21 (7)	0 (0)	21
t10p5	34 (6.8)	121 (41.9)	155	122 (24.4)	14 (4.8)	136	20 (4)	1 (0.4)	21
t10p7	45 (6.4)	209 (74.9)	254	169 (24.1)	14 (5.0)	183	39 (5.6)	0 (0)	39
t10ke0	170 (56.7)	6 (13.6)	176	2 (0.67)	0 (0)	2	40 (13.3)	0 (0)	40
t10ke05	22 (7.3)	50 (29.4)	72	79 (26.3)	4 (2.4)	83	15 (5)	0 (0)	15
t8cr	216 (72)	2 (100)	218	9 (3)	0 (0)	9	33 (11)	0 (0)	33
t9cr	217 (72.3)	3 (21.4)	220	6 (2)	0 (0)	6	33 (11)	0 (0)	33
t10cr	169 (56.3)	6 (17.6)	175	6 (2)	1 (2.9)	7	28 (9.3)	0 (0)	28
t11cr	160 (53.3)	8 (17.0)	168	2 (0.67)	0 (0)	2	26 (8.7)	0 (0)	26
t7cr2	214 (71.3)	4 (40)	218	16 (5.3)	0 (0)	16	33 (11)	0 (0)	33
t8cr2	180 (60)	9 (24.3)	189	8 (2.7)	0 (0)	8	33 (11)	0 (0)	33
t9cr2	151 (50.3)	7 (12.7)	158	3 (1)	0 (0)	3	33 (11)	0 (0)	33
t10cr2	101 (33.7)	20 (17.2)	121	6 (2)	1 (0.86)	7	28 (9.3)	0 (0)	28

NOTE. — Numbers of planets which are ejected from the system, collided with the central star, and merged with another planet, before and after the gas dissipation times  $\tau_{GD}$ , as well as throughout the simulations. Large number of collisions before  $\tau_{GD}$  indicates efficient planet migration, while the large number of ejections indicates dynamical instability. The percentages of planets in more than two-planet systems which are ejected/collided/merged are shown inside the bracket.

Murray, C. D. & Dermott, S. F. 1999, Solar system dynamics (Solar system dynamics by Murray, C. D., 1999)  
Ogilvie, G. I. & Lubow, S. H. 2002, MNRAS, 330, 950  
Rasio, F. A., Tout, C. A., Lubow, S. H., & Livio, M. 1996, ApJ, 470, 1187  
Raymond, S. N., Barnes, R., Armitage, P. J., & Gorelick, N. 2008, ApJL, 687, L107  
Shakura, N. I. & Sunyaev, R. A. 1973, A&A, 24, 337  
Sicilia-Aguilar, A., Hartmann, L. W., Fürész, G., Henning, T., Dullemond, C., & Brandner, W. 2006, AJ, 132, 2135  
Simon, M. & Prato, L. 1995, ApJ, 450, 824  
Tanigawa, T. & Watanabe, S.-i. 2002, ApJ, 580, 506  
Thommes, E. W. 2005, ApJ, 626, 1033

Thommes, E. W., Matsumura, S., & Rasio, F. A. 2008, Science, 321, 814  
Udry, S. & Santos, N. C. 2007, ARA&A, 45, 397  
Ward, W. R. 1997, Icarus, 126, 261  
Weidenschilling, S. J. & Marzari, F. 1996, Nature, 384, 619  
Wisdom, J. & Holman, M. 1991, AJ, 102, 1528  
Wittenmyer, R. A., Endl, M., & Cochran, W. D. 2007, ApJ, 654, 625  
Wright, J. T., Marcy, G. W., Fischer, D. A., Butler, R. P., Vogt, S. S., Tinney, C. G., Jones, H. R. A., Carter, B. D., Johnson, J. A., McCarthy, C., & Apps, K. 2007, ApJ, 657, 533

TABLE 3  
THE K-S TEST FOR  $a$  AND  $e$  DISTRIBUTIONS

Set No.	$\tau_{GD}$ and $\tau_{fin}$		Semi-major axis $a$				Eccentricity $e$					
	D	P	$\tau_{GD}$ and Obs D	P	$\tau_{fin}$ and Obs D	P	$\tau_{GD}$ and $\tau_{fin}$ D	P	$\tau_{GD}$ and Obs D	P	$\tau_{fin}$ and Obs D	P
S50	0.268	0.235	0.592	0	0.381	0	0.409	0.0137	0.483	0	0.209	0.370
S40	0.101	0.784	0.459	0	0.407	0	0.275	0	0.464	0	0.236	0
S30	0.123	0.131	0.342	0	0.259	0	0.242	0	0.551	0	0.420	0
tgd2	0.0384	0.986	0.0853	0.407	0.0768	0.548	0.0826	0.295	0.648	0	0.638	0
tgd3	0.0888	0.428	0.286	0	0.211	0	0.154	0.0203	0.627	0	0.513	0
tgd4	0.0818	0.966	0.475	0	0.468	0	0.141	0.456	0.522	0	0.409	0
t9	0.0742	0.993	0.459	0	0.430	0	0.200	0.154	0.519	0	0.447	0
t10	0.0884	0.599	0.281	0	0.216	0	0.145	0.0833	0.586	0	0.476	0
t11	0.0873	0.335	0.134	0.0467	0.0678	0.764	0.139	0.0219	0.638	0	0.521	0
t13	0.0431	0.990	0.303	0	0.285	0	0.0675	0.724	0.662	0	0.649	0
t10p5	0.0582	0.731	0.145	0.0205	0.104	0.201	0.268	0	0.658	0	0.431	0
t10p7	0.105	0.240	0.176	0	0.227	0	0.303	0	0.631	0	0.352	0
t10ke0	0.106	0.738	0.0974	0.705	0.146	0.149	0.0900	0.890	0.146	0.219	0.127	0.279
t10ke05	0.157	0.0684	0.289	0	0.270	0	0.157	0.0684	0.566	0	0.417	0
t8cr	0.333	0.810	0.269	0.722	0.269	0.722	0.500	0.318	0.362	0.349	0.547	0.0383
t9cr	0.164	0.757	0.199	0.263	0.265	0.0273	0.136	0.917	0.213	0.196	0.165	0.372
t10cr	0.0927	0.927	0.188	0.0719	0.158	0.144	0.108	0.813	0.252	0	0.189	0.0464
t11cr	0.107	0.731	0.222	0.0113	0.148	0.145	0.0996	0.809	0.194	0.0372	0.119	0.368
t7cr2	0.172	0.825	0.147	0.740	0.231	0.154	0.249	0.381	0.260	0.108	0.191	0.349
t8cr2	0.0930	0.962	0.123	0.502	0.160	0.228	0.135	0.659	0.0818	0.923	0.101	0.782
t9cr2	0.0584	0.998	0.0728	0.932	0.0702	0.910	0.0578	0.998	0.130	0.308	0.141	0.158
t10cr2	0.0818	0.821	0.248	0	0.238	0	0.0788	0.854	0.118	0.290	0.0870	0.639

NOTE. — The results of the K-S test for semimajor axis and eccentricity. We compare the simulated results at  $\tau_{GD}$  with  $\tau_{fin}$  (10 Myr for Set tgd2, tgd3, and tgd4 and 100 Myr for the others), as well as the simulated results at  $\tau_{fin}$  with observed planets between 0.2 AU  $\lesssim a \lesssim$  6 AU. The maximum deviation between two cumulative fraction curves D, and the corresponding probability P are shown for each comparison. We reject the null hypothesis for P less than 0.1. Here, the null hypothesis is that the pair of samples used in the test is drawn from the same distribution. The comparison for Set t7 is not included since most planets are lost before  $\tau_{GD}$ .